Noname manuscript No.
(will be inserted by the editor)

Sparse-data Based 3D Surface Reconstruction for Cartoon and Map

Bin Wu · Xue-Cheng Tai · Talal Rahman

the date of receipt and acceptance should be inserted later

Abstract A model combining the first-order and the second-order variational regularizations for the purpose of 3D surface reconstruction based on 2D sparse data is proposed. The model includes a hybrid fidelity constraint which allows the initial conditions to be switched flexibly between vectors and elevations. A numerical algorithm based on the augmented Lagrangian method is also proposed. The numerical experiments are presented, showing its excellent performance both in designing cartoon characters, as well as in recovering oriented three dimensional maps from contours or points with elevation information.

1 Introduction

Image processing has a strong influence and impact on our world, finding applications in almost all areas from nanophysics to astrophysics, from biology to social sciences, from robotics to smart phone applications, etc. 3D surface reconstruction from sparse data is both a challenging and an interesting image processing task.

One area of application of the surface reconstruction has been the sketch based 3D design, which has attracted much attention, cf. [1–5], because it is intuitive and effective, particularly in applications like cartoon and game design. To a sketch based method, the only known informations are information given on sparse lines, for instance in the form of contours [2], without specifying the heights, or in

Bin Wu
Department of Mathematics, University of Bergen, Allégaten 41, 5007 Bergen, Norway, and Department of Computer Science, Electrical Engineering and Mathematical Sciences, Western Norway University of Applied Sciences, Inndalsveien 28, 5063 Bergen, Norway
E-mail: b.wu@uib.no

Xue-Cheng Tai
Department of Mathematics, University of Bergen, Allégaten 41, 5007 Bergen, Norway
E-mail: xue-cheng.tai@uib.no

Talal Rahman
Department of Computer Science, Electrical Engineering and Mathematical Sciences, Western Norway University of Applied Sciences, Inndalsveien 28, 5063 Bergen, Norway
E-mail: talal.rahman@hvl.no

the form of complex sketches with elevation [3], or structured annotations [6]. However, the methods proposed in those papers are limited in their capabilities in reconstructing structures with crease. The crease can be added artificially [7]. However, a simple and automatic method is still necessay when the task becomes large, complex and computationally intensive. Recently, to this end, there is a method been proposed [8,9] which interpolates the normal vectors under curl-free constraint and then reconstructs the 3D surface based on the obtained vector field. The method [8,9] is based on the previous work on surface reconstruction from surface gradients [10–17] and inspired by TV-Stokes method [18–22] where actually the curl-free constraint comes from. The main difference of this method [8, 9] compared to the other two-step methods [15,23] is that, instead of the Laplace operator, an TV regularizer is employed which is better in edge preserving. In addition, a more physical constraint, the curl-free constraint is introduced by the method. The numerical results show an excellent performance in preserving edges and crease structures.

Another area of application has been the 3D surface reconstruction based only on height values (contours) or both height values and vectors. The height values are needed because the reconstructed surfaces for such applications are expected to be as precise as possible to the ground truth, e.g. the digital elevation maps and data compression. One way is to use explicit parameterization of given contours with subsequent pointwise matching and interpolation [24–26]. For such models, the parametrization may be difficult and expensive to compute, and the loss of continuity of slope across contours is a challenge. Another way is to treat the expected surface as a function over the considered domain. A renowned model is the absolutely minimizing Lipschitz extension (AMLE) interpolation model, see [27, 28], based on the PDE theory. The AMLE has a drawback in interpolating slopes. To overcome, one can rely on high-order differential operators or regularizations [29–33]. The method addressed in [33] introduces a third order anisotropic regularization together with a way to find an auxiliary vector field. The method results in clear surfaces with anisotropic features.

It is however desirable to recover the 3D surface with enough precision at the same time to be able to adjust the shape of the reconstructed surface by tuning vectors. For instance in case of data compression, it may be helpful to store vectors (relative positions) along with sparse elevations instead of single the sparse elevations for correct representations. The aim of this paper is to propose a versatile model incorporating both height and vector information in one place. We thus propose a one-step model with a combination of first-order and second-order variational regularizations under a hybrid fidelity constraint consisting of both elevation and normal vectors. The main contributions of our research can be summarized as follows:

- The model allows for adjusting normal vectors intuitively and a more precise representation of the elevations. It preserves both structures and details.
- A fast and efficient numerical algorithm based on the augmented Lagrangian method [34–36] is proposed which can be used for 3D surface reconstruction of cartoon and digital map based on very sparse 2D input data.

The paper is organized as follows. In section 2, we propose our model with a first-order and a second-order regularizations and a hybrid constraint. In section 3, we present numerical method based on augmented Lagrangian. Numerical experi-

ments on cartoon design and three dimensional map reconstructions are presented in section 4. Finally, in section 5, we give our conclusion.

2 Proposed Model

We first explain the model presented in [8,9] before we propose ours. We define the surface as the graph of I given by the points $(x, y, I(x, y)) \subset \mathbb{R}^3$ in the space, where I is a function of the coordinates x and y over a two dimensional domain $\Omega \subset \mathbb{R}^2$. The normal vector to the surface or the graph is then given by $(-\partial_x I, -\partial_y I, 1)$. Projecting it to the $xy-$plane, we get the 2D normal vectors as $(-\partial_x I, -\partial_y I)$. Because I is a scalar-valued function, the curl of the gradient of I must be zero. Based on this, a curl-free model has been proposed in [8,9]. They first interpolated the normal vector $\mathbf{n} := (\partial_x I, \partial_y I)$ by solving the following constrained minimization problem

$$\min_{\mathbf{n}} \left\{ \int_{\Omega} (1-g)|\nabla \mathbf{n}|_F + g|\nabla \mathbf{n}|_F^2 + \eta \int_{\Gamma} |\mathbf{n} - \mathbf{n}^*| \right\}, \tag{1}$$

subject to the curl free condition

$$\nabla \times \mathbf{n} = 0,$$

where $\mathbf{n}^*$ is the known normal vector along some given sparse lines or strokes Γ, g is the parameter for a convex combination of the TV and the H^1 norm, and η is the parameter to balance between the regularization terms and the fidelity term. We note that $|\cdot|_F$ is used to denote the standard Frobenius norm [38]. The height map I is then reconstructed by solving the following minimization problem

$$\min_{I} \left\{ \int_{\Omega} (1-h)|\nabla I - \mathbf{n}| + h|\nabla I - \mathbf{n}|^2 + \xi \int_{\Sigma} |I - I_0| \right\}, \tag{2}$$

where $\mathbf{n}$ is the normal vector field obtained from the first minimization step, I_0 is the known elevation along some given sparse lines or strokes Σ, h is the parameter for a convex combination of TV and H^1 norms, ξ is the parameter to balance between the regularization terms and the fidelity term.

It is obvious that reconstructing a 3D surface would require both constraints, the one on the normal vector $\mathbf{n}$ and the one on the height I, corresponding to the fidelity terms of (1) and (2). However, since the model above is not coupled, it is hard to satisfy both constraints simultaneously, and therefore the resulting surface may deviate from the surface actually being sought.

We therefore propose the following one-step model including both the height and the normal vector constraint, that is the hybrid constraint.

$$\min_{I} \left\{ \int_{\Omega} g|\nabla(\nabla I)|_F + h|\nabla I| + \int_{\Gamma} \eta|\nabla I - \mathbf{n}^0| + \int_{\Sigma} \theta|I - I^0| \right\}, \tag{3}$$

where h and g are parameters for the first and the second variational regularizations, respectively. We note here that because our model is of second order, it naturally satisfies the curl free condition.

3 Augmented Lagrangian Method

For the numerical solution of the problem (4), we derive an augmented Lagrangian method, cf. [34]. Augmented Lagrangian method is preferred because it is in general fast and efficient; for its use in image processing, we refer to e.g. [35,36].

In order to be able to define our entire minimization problem over the whole domain, we replace the two fidelity parameters η and θ with the following parameters,

$$\hat{\eta} = \begin{cases} \eta, & \text{on } \Gamma \\ 0, & \text{in } \Omega\backslash\Gamma, \end{cases} \qquad \text{and} \quad \hat{\theta} = \begin{cases} \theta, & \text{on } \Sigma \\ 0, & \text{in } \Omega\backslash\Sigma. \end{cases}$$

We get our model (3) reformulated as follows,

$$\min_I \left\{ \int_\Omega g|\nabla(\nabla I)|_F + h|\nabla I| + \hat{\eta}|\nabla I - \mathbf{n}^0| + \hat{\theta}|I - I^0| \right\}. \tag{4}$$

We shall introduce some auxiliary variables and turn the above minimization problem into an equivalent constrained minimization problem. For the four L_1-norm terms in the above functional, introducing one new variable to each, we get four new variables $\mathbf{Q} := \nabla\mathbf{E}$, $\mathbf{P} := \nabla I$, $\mathbf{C} := \mathbf{P}$, and $S := I$, corresponding to $|\nabla(\nabla I)|_F$, $|\nabla I|$, $|\nabla I - \mathbf{n}^0|$, and $|I - I^0|$, respectively. In addition, for the term $|\nabla(\nabla I)|_F$, we introduce another variable $\mathbf{E} := \mathbf{P}$ in order to avoid dealing with high order terms. The unconstrained minimization problem (4) is then converted to an equivalent constrained optimization problem as:

$$\min_{\mathbf{Q},\mathbf{P},\mathbf{C},S} \left\{ \int_\Omega g|\mathbf{Q}|_F + h|\mathbf{P}| + \hat{\eta}|\mathbf{C} - \mathbf{n}^0| + \hat{\theta}|S - I^0| \right\}$$

such that

$$\mathbf{P} - \nabla I = 0; \quad \mathbf{E} - \mathbf{P} = 0; \quad \mathbf{Q} - \nabla\mathbf{E} = 0; \quad S - I = 0; \quad \text{and} \quad \mathbf{C} - \mathbf{P} = 0,$$

where $\mathbf{C}, \mathbf{E}, \mathbf{P} \in \mathbb{R}^2$ are 2-dimensional vectors, and $\mathbf{Q} \in \mathbb{R}^{2\times 2}$ is a 2-by-2 matrix. Using Lagrange multipliers and adding penalty terms for each condition, we get the following augmented Lagrangian functional

$$\begin{aligned} \mathcal{L}\left(_{\Lambda_Q,\Lambda_P,\Lambda_C,\lambda_S,\Lambda_E}^{\mathbf{Q},\mathbf{P},\mathbf{C},S,I,\mathbf{E};}\right) = \int_\Omega & g|\mathbf{Q}|_F + h|\mathbf{P}| + \hat{\eta}|\mathbf{C} - \mathbf{n}^0| + \hat{\theta}|S - I^0| \\ & + \Lambda_Q \cdot (\mathbf{Q} - \nabla\mathbf{E}) + \frac{c_Q}{2}|\mathbf{Q} - \nabla\mathbf{E}|_F^2 \\ & + \Lambda_P \cdot (\mathbf{P} - \nabla I) + \frac{c_P}{2}|\mathbf{P} - \nabla I|^2 \\ & + \Lambda_C \cdot (\mathbf{C} - \mathbf{P}) + \frac{c_C}{2}|\mathbf{C} - \mathbf{P}|^2 \\ & + \lambda_S \cdot (S - I) + \frac{c_S}{2}|S - I|^2 \\ & + \Lambda_E \cdot (\mathbf{E} - \mathbf{P}) + \frac{c_E}{2}|\mathbf{E} - \mathbf{P}|^2, \end{aligned}$$

where Λ_Q, Λ_P, Λ_C, λ_S and Λ_E are Lagrange multipliers, c_Q, c_P, c_C, c_S and c_E are positive penalty parameters. That is, the augmented Lagrangian method is to seek a saddle point of the following problem:

$$\min_{\mathbf{Q},\mathbf{P},\mathbf{C},S,I,\mathbf{E}} \max_{\Lambda_Q,\Lambda_P,\Lambda_C,\lambda_S,\Lambda_E} \mathcal{L}\left(_{\Lambda_Q,\Lambda_P,\Lambda_C,\lambda_S,\Lambda_E}^{\mathbf{Q},\mathbf{P},\mathbf{C},S,I,\mathbf{E};}\right). \tag{5}$$

For the solution we solve its associated system of optimality conditions with an iterative procedure, see Algorithm 1 and Algorithm 2. For the sake of convenience, we use $\Lambda := (\lambda_S, \Lambda_P, \Lambda_C, \Lambda_Q, \Lambda_E)$ to denote the Lagrange multipliers.

Algorithm 1: The augmented Lagrangian for (5)

Set $k = 0$;
Initialize $\mathbf{Q}^0$, $\mathbf{P}^0$, $\mathbf{C}^0$, S^0, I^0, $\mathbf{E}^0$ and Λ^0 ;
while *not converged* **do**
Set $k = k + 1$;
Given Λ^{k-1}, solve the minimization problem:

$$(\mathbf{Q}^k, \mathbf{P}^k, \mathbf{C}^k, S^k, I^k, \mathbf{E}^k) = \arg \min_{\mathbf{Q},\mathbf{P},\mathbf{C},S,I,\mathbf{E}} \mathcal{L}(\mathbf{Q}, \mathbf{P}, \mathbf{C}, S, I, \mathbf{E}; \Lambda^{k-1}); \quad (6)$$

Update the Lagrange multipliers:

$$\begin{aligned} \lambda_S^k &= \lambda_S^{k-1} + c_S(S^k - I^k); & \Lambda_P^k &= \Lambda_P^{k-1} + c_P(\mathbf{P}^k - \nabla I^k); \\ \Lambda_C^k &= \Lambda_C^{k-1} + c_C(\mathbf{C}^k - \mathbf{P}^k); & \Lambda_Q^k &= \Lambda_Q^{k-1} + c_Q(\mathbf{Q}^k - \nabla(\mathbf{E}^k)); \\ \Lambda_E^k &= \Lambda_E^{k-1} + c_E(\mathbf{E}^k - \mathbf{P}^k); \end{aligned}$$

end

Algorithm 2: Alternating minimization for (6)

Set $l = 0$;
Initialize $\mathbf{Q}^{k,0} = \mathbf{Q}^{k-1}$; $\mathbf{P}^{k,0} = \mathbf{P}^{k-1}$; $\mathbf{C}^{k,0} = \mathbf{C}^{k-1}$; $S^{k,0} = S^{k-1}$; $I^{k,0} = I^{k-1}$; $\mathbf{E}^{k,0} = \mathbf{E}^{k-1}$;
while *not converged and* $l < L$ **do**
Solve the sub-minimization problems:

$$\begin{aligned} \mathbf{Q}^{k,l+1} &= \arg\min_{\mathbf{Q}} \mathcal{L}(\mathbf{Q}, \mathbf{P}^{k,l}, \mathbf{C}^{k,l}, S^{k,l}, I^{k,l}, \mathbf{E}^{k,l}; \Lambda^{k-1}); \\ \mathbf{P}^{k,l+1} &= \arg\min_{\mathbf{P}} \mathcal{L}(\mathbf{Q}^{k,l+1}, \mathbf{P}, \mathbf{C}^{k,l}, S^{k,l}, I^{k,l}, \mathbf{E}^{k,l}; \Lambda^{k-1}); \\ \mathbf{C}^{k,l+1} &= \arg\min_{\mathbf{C}} \mathcal{L}(\mathbf{Q}^{k,l+1}, \mathbf{P}^{k,l+1}, \mathbf{C}, S^{k,l}, I^{k,l}, \mathbf{E}^{k,l}; \Lambda^{k-1}); \\ S^{k,l+1} &= \arg\min_{S} \mathcal{L}(\mathbf{Q}^{k,l+1}, \mathbf{P}^{k,l+1}, \mathbf{C}^{k,l+1}, S, I^{k,l}, \mathbf{E}^{k,l}; \Lambda^{k-1}); \\ I^{k,l+1} &= \arg\min_{I} \mathcal{L}(\mathbf{Q}^{k,l+1}, \mathbf{P}^{k,l+1}, \mathbf{C}^{k,l+1}, S^{k,l+1}, I, \mathbf{E}^{k,l}; \Lambda^{k-1}); \\ \mathbf{E}^{k,l+1} &= \arg\min_{\mathbf{E}} \mathcal{L}(\mathbf{Q}^{k,l+1}, \mathbf{P}^{k,l+1}, \mathbf{C}^{k,l+1}, S^{k,l+1}, I^{k,l+1}, \mathbf{E}; \Lambda^{k-1}); \end{aligned}$$

Set $l = l + 1$;
end
Set $(\mathbf{Q}^k, \mathbf{P}^k, \mathbf{C}^k, S^k, I^k, \mathbf{E}^k) = (\mathbf{Q}^{k,L}, \mathbf{P}^{k,L}, \mathbf{C}^{k,L}, S^{k,L}, I^{k,L}, \mathbf{E}^{k,L})$.

Because the variables $\mathbf{Q}$, $\mathbf{P}$, $\mathbf{C}$, S, I and $\mathbf{E}$ in $\mathcal{L}(\mathbf{Q}, \mathbf{P}, \mathbf{C}, S, I, \mathbf{E}; \Lambda^{k-1})$ are coupled together in the minimization problem (6), it is difficult to solve them simultane-

ously. We split the minimization problem into six sub minimization problems, and solve them alternatively to convergence, see Algorithm 2.
The six sub-minimization problems can be formulated in a more specific and clearly way as in the following:

- The **Q**-subproblem needs to solve:

$$\mathbf{Q}^\star = \arg\ \min_{\mathbf{Q}} \int_\Omega g|\mathbf{Q}|_F + \Lambda_Q \cdot \mathbf{Q} + \frac{c_Q}{2}|\mathbf{Q} - \nabla\mathbf{E}|_F^2. \tag{7}$$

- With $\tilde{\Lambda} := \Lambda_P - \Lambda_E - \Lambda_C$, the **P**-subproblem needs to solve:

$$\mathbf{P}^\star = \arg\ \min_{\mathbf{P}} \int_\Omega h|\mathbf{P}| + \tilde{\Lambda} \cdot \mathbf{P} + \frac{c_P}{2}|\mathbf{P} - \nabla I|^2 + \frac{c_E}{2}|\mathbf{E} - \mathbf{P}|^2 + \frac{c_C}{2}|\mathbf{C} - \mathbf{P}|^2. \tag{8}$$

- The **C**-subproblem needs to solve:

$$\mathbf{C}^\star = \arg\ \min_{\mathbf{C}} \int_\Omega \Lambda_C \cdot \mathbf{C} + \frac{c_C}{2}|\mathbf{C} - \mathbf{P}|^2 + \hat{\eta}|\mathbf{C} - \mathbf{n}^0|. \tag{9}$$

- The S-subproblem needs to solve:

$$S^\star = \arg\ \min_{S} \int_\Omega \lambda_S \cdot S + \frac{c_S}{2}|S - I|^2 + \hat{\theta}|S - I^0|. \tag{10}$$

- The I-subproblem needs to solve:

$$I^\star = \arg\ \min_{I} \int_\Omega -\Lambda_P \cdot \nabla I + \frac{c_P}{2}|\mathbf{P} - \nabla I|^2 - \lambda_S \cdot I + \frac{c_S}{2}|S - I|^2. \tag{11}$$

- The **E**-subproblem needs to solve:

$$\mathbf{E}^\star = \arg\ \min_{\mathbf{E}} \int_\Omega \Lambda_E \cdot \mathbf{E} + \frac{c_E}{2}|\mathbf{E} - \mathbf{P}|^2 - \Lambda_q \cdot \nabla\mathbf{E} + \frac{c_Q}{2}|\mathbf{Q} - \nabla\mathbf{E}|_F^2. \tag{12}$$

For the first four sub-minimization problems, we can find closed form solutions. Each problem has one L_1-norm term, and either one or more than one quadratic terms in its objective functional. Such problems can be solved using either a sub-gradient method, cf. [37], or a geometric method, cf. [36]. However, we will use a different approach to get the close form solutions in this work. We propose a simpler approach which is based on the optimality condition of the minimization functionals, i.e. the Euler-Lagrange equations. More details on this will be given below, see also Definition 3.1. For the last two sub-minimization problems, we solve them by the discrete cosine transform, see Remark 3.1.

Definition 3.1 If A and B are two matrices such that $A = \lambda B$ for some non-negative real number λ, then we say that A is compatible with B. It is easy to see that $A/|A|_F = B/|B|_F$.

In the following, we elaborate more on the details in getting close form solutions or design fast solvers for the subproblems.

3.1 Solving the Q-subproblem (7):

The optimality condition, that is the Euler-Lagrange equation, for the Q-subproblem (7) is as follows

$$\frac{g}{c_Q}\frac{\mathbf{Q}^\star}{|\mathbf{Q}^\star|_F} + \mathbf{Q}^\star = \nabla\mathbf{E} - \frac{\Lambda_Q}{c_Q}.$$

Since g and c_Q are both positive numbers, the matrices $\mathbf{Q}^\star$ and $(\nabla\mathbf{E} - \frac{\Lambda_Q}{c_Q})$ are both compatible in the sense of Definition 3.1, according to which, we can replace $\mathbf{Q}^\star/|\mathbf{Q}^\star|_F$ with $(\nabla\mathbf{E} - \frac{\Lambda_Q}{c_Q})/|\nabla\mathbf{E} - \frac{\Lambda_Q}{c_Q}|_F$. Now moving it to the right hand side, we get

$$\mathbf{Q}^\star = \left(1 - \frac{g}{c_Q|\nabla\mathbf{E} - \frac{\Lambda_Q}{c_Q}|_F}\right)\left(\nabla\mathbf{E} - \frac{\Lambda_Q}{c_Q}\right).$$

Again since $\mathbf{Q}^\star$ and $\nabla\mathbf{E} - \frac{\Lambda_Q}{c_Q}$ are compatible, the coefficient on the right hand side, that is $\left(1 - \frac{g}{c_Q|\nabla\mathbf{E} - \frac{\Lambda_Q}{c_Q}|_F}\right)$, must be non-negative, and hence

$$\mathbf{Q}^\star = \max\left\{0, 1 - \frac{g}{c_Q|\nabla\mathbf{E} - \frac{\Lambda_Q}{c_Q}|_F}\right\}\left(\nabla\mathbf{E} - \frac{\Lambda_Q}{c_Q}\right).$$

With the derivation given above, we have shown an easy way to get a close form solution for the subproblem. We shall use similar techniques to get close form solutions for some of the other subproblems.

3.2 Solving the P-subproblem (8):

The corresponding Euler-Lagrange equation for the P-subproblem (8) is the following,

$$\frac{h}{c_P + c_E + c_C}\frac{\mathbf{P}^\star}{|\mathbf{P}^\star|} + \mathbf{P}^\star = \frac{c_P\nabla I + c_E\mathbf{E} + c_C\mathbf{C}}{c_P + c_E + c_C} - \frac{\tilde{\Lambda}}{c_P + c_E + c_C}.$$

Use $\mathbf{X}$ to denote $\frac{c_P\nabla I + c_E\mathbf{E} + c_C\mathbf{C}}{c_P + c_E + c_C} - \frac{\tilde{\Lambda}}{c_P + c_E + c_C}$. In the same way as before, since h, c_P, c_E and c_C are positive numbers, both vectors $\mathbf{P}^\star$ and $\mathbf{X}$ are compatible (cf. Definition 3.1). Accordingly, we replace $\mathbf{P}^\star/|\mathbf{P}^\star|$ with $\mathbf{X}/|\mathbf{X}|$, and move it to the right hand side, to get

$$\mathbf{P}^\star = \left(1 - \frac{h}{(c_P + c_E + c_C)|\mathbf{X}|}\right)\mathbf{X}.$$

Again since $\mathbf{P}^\star$ and $\mathbf{X}$ are compatible, the coefficient $\left(1 - \frac{h}{(c_P + c_E + c_C)|\mathbf{X}|}\right)$ must be non-negative. Hence

$$\mathbf{P}^\star = \max\left\{0, 1 - \frac{h}{(c_P + c_E + c_C)|\mathbf{X}|}\right\}\mathbf{X}.$$

3.3 Solving the C-subproblem (9):

The corresponding Euler-Lagrange equation is the following,

$$\mathbf{C}^\star - \mathbf{n}^0 + \frac{\hat{\eta}}{c_C}\frac{\mathbf{C}^\star - \mathbf{n}^0}{|\mathbf{C}^\star - \mathbf{n}^0|} = \mathbf{P} - \mathbf{n}^0 - \frac{\Lambda_C}{c_C}.$$

Since $\hat{\eta}$ and c_C are both positive numbers, it follows that both vectors $\mathbf{C}^\star - \mathbf{n}^0$ and $\mathbf{P} - \mathbf{n}^0 - \frac{\Lambda_C}{c_C}$ are compatible (cf. Definition 3.1). Accordingly, we replace $(\mathbf{C}^\star - \mathbf{n}^0)/|\mathbf{C}^\star - \mathbf{n}^0|$ with $(\mathbf{P} - \mathbf{n}^0 - \frac{\Lambda_C}{c_C})/|\mathbf{P} - \mathbf{n}^0 - \frac{\Lambda_C}{c_C}|$, and move it to the right hand side, to obtain

$$\mathbf{C}^\star - \mathbf{n}^0 = \left(1 - \frac{\hat{\eta}}{c_C|\mathbf{P} - \mathbf{n}^0 - \frac{\Lambda_C}{c_C}|}\right)(\mathbf{P} - \mathbf{n}^0 - \frac{\Lambda_C}{c_C}).$$

Again since $\mathbf{C}^\star - \mathbf{n}^0$ and $\mathbf{P} - \mathbf{n}^0 - \frac{\Lambda_C}{c_C}$ are compatible, the coefficient $\left(1 - \frac{\hat{\eta}}{c_C|\mathbf{P}-\mathbf{n}^0-\frac{\Lambda_C}{c_C}|}\right)$ must be non-negative. Hence

$$\mathbf{C}^\star = \mathbf{n}^0 + \max\left\{0, 1 - \frac{\hat{\eta}}{c_C|\mathbf{P} - \mathbf{n}^0 - \frac{\Lambda_C}{c_C}|}\right\}\left(\mathbf{P} - \mathbf{n}^0 - \frac{\Lambda_C}{c_C}\right).$$

3.4 Solving the S-subproblem (10):

The Euler-Lagrange equation is the following,

$$S^\star - I^0 + \frac{\hat{\theta}}{c_S}\frac{S^\star - I^0}{|S^\star - I^0|} = I - I^0 - \frac{\lambda_S}{c_S}.$$

Again using the fact that $\hat{\theta}$ and c_S are both positive numbers, it follows that $S^\star - I^0$ and $I - I^0 - \frac{\lambda_S}{c_S}$ have the same sign. Replacing $(S^\star - I^0)/|S^\star - I^0|$ with $(I - I^0 - \frac{\lambda_S}{c_S})/|I - I^0 - \frac{\lambda_S}{c_S}|$, and moving it to the right hand side, we obtain

$$S^\star - I^0 = \left(1 - \frac{\hat{\theta}}{c_S|I - I^0 - \frac{\lambda_S}{c_S}|}\right)\left(I - I^0 - \frac{\lambda_S}{c_S}\right).$$

Because $S^\star - I^0$ and $I - I^0 - \frac{\lambda_S}{c_S}$ have the same sign, the coefficient $\left(1 - \frac{\hat{\theta}}{c_S|I-I^0-\frac{\lambda_S}{c_S}|}\right)$ must be non-negative. Therefore

$$S^\star = I^0 + \max\left\{0, 1 - \frac{\hat{\theta}}{c_S|I - I^0 - \frac{\lambda_S}{c_S}|}\right\}\left(I - I^0 - \frac{\lambda_S}{c_S}\right).$$

3.5 Solving the I-subproblem (11):

The Euler-Lagrange equation is the following inhomogeneous modified Helmholtz equation,

$$\nabla \cdot \nabla I^\star - \frac{c_S}{c_P} I^\star = \nabla \cdot \mathbf{P} + \frac{1}{c_P} \nabla \cdot \Lambda_P - \frac{c_S}{c_P} S - \frac{1}{c_P} \lambda_S,$$

with the Neumann boundary condition,

$$\nabla I^\star \cdot \nu = (\mathbf{P} + \frac{1}{c_P} \Lambda_P) \cdot \nu,$$

where the ν denotes the outward unit normal vector on the boundary of the domain. The Euler-Lagrange equation, with the boundary condition, is solved by the discrete cosine transform. Details are given in Remark 3.1.

3.6 Solving the E-subproblem (12):

The corresponding Euler-Lagrange equation is the following,

$$\nabla \cdot \nabla \mathbf{E}^\star - \frac{c_E}{c_Q} \mathbf{E}^\star = \frac{1}{c_Q} \Lambda_E - \frac{c_E}{c_Q} \mathbf{P} + \frac{1}{c_Q} \nabla \cdot \Lambda_Q + \nabla \cdot \mathbf{Q},$$

which is a set of two inhomogeneous modified Helmholtz equations, one equation for each component of $\mathbf{E} = (E_1, E_2)$, and corresponding Neumann boundary conditions,

$$\nabla E_1 \cdot \nu = (\mathbf{Q}_1 + \frac{1}{c_Q} \Lambda_{Q1}) \cdot \nu,$$

$$\nabla E_2 \cdot \nu = (\mathbf{Q}_2 + \frac{1}{c_Q} \Lambda_{Q2}) \cdot \nu,$$

where $\mathbf{Q}_1$ and $\mathbf{Q}_2$ are the row vectors of the matrix $\mathbf{Q}$, and Λ_{Q1} and Λ_{Q2} are corresponding Lagrange multipliers, respectively. ν is the outward unit normal on the boundary of the domain. Each equation is solved in the same way as in the I-subproblem, cf. Remark 3.1.

Remark 3.1 The last two sub-minimization problems, each reduces to solve a partial differential equation of the form

$$\triangle u(x, y) - \lambda u(x, y) = F(x, y),$$

with a Neumann boundary condition and λ a non-negative number, also known as the inhomogeneous modified Helmholtz equation. A fast solver based on discrete cosine transform similar for the Poisson equation, cf. [39,40], is developed as the following treatment.

Using the singular value decomposition, the discrete Laplace operator

$$\begin{bmatrix} -1 & 1 & & & \\ 1 & -2 & 1 & & \\ & \ddots & \ddots & \ddots & \\ & & 1 & -2 & 1 \\ & & & 1 & -1 \end{bmatrix}$$

takes the form of [40],

$$-C^\top \begin{bmatrix} 0 & \\ & \Sigma^2 \end{bmatrix} C,$$

where C is the $N \times N$ discrete cosine transform matrix and $\Sigma = \mathrm{diag}(\sigma_1, \cdots, \sigma_{N-1})$ is the diagonal matrix with its diagonal entries representing the singular values $\sigma_k = 2 \sin \dfrac{\pi k}{2N}$ for $k = 1, 2, \cdots, N-1$. Now using this the discrete (matrix) formulation of the inhomogeneous modified Helmholtz equation then reads

$$-uC^\top \begin{bmatrix} 0 & \\ & \Sigma_x^2 \end{bmatrix} C - C^\top \begin{bmatrix} 0 & \\ & \Sigma_y^2 \end{bmatrix} Cu - \lambda u = F.$$

A further transformation using $\tilde{u} = CuC^\top$ and $\tilde{F} = CFC^\top$, results in

$$-\tilde{u} \begin{bmatrix} 0 & \\ & \Sigma_x^2 \end{bmatrix} - \begin{bmatrix} 0 & \\ & \Sigma_y^2 \end{bmatrix} \tilde{u} - \lambda \tilde{u} = \tilde{F}.$$

The solution of the above equation can be obtained by a direct entrywise division due to the linearity of the equation as well as the non-singularity of the coefficient matrix, and is formulated as

$$\tilde{u} = \tilde{F}./M,$$

where ./ denotes the entrywise division and M is the $N \times N$ coefficient matrix defined as

$$M = -\begin{bmatrix} 0 & \sigma_{1,x}^2 & \cdots & \sigma_{N-2,x}^2 & \sigma_{N-1,x}^2 \\ \sigma_{1,y}^2 & \sigma_{1,x}^2 + \sigma_{1,y}^2 & \cdots & \sigma_{N-2,x}^2 + \sigma_{1,y}^2 & \sigma_{N-1,x}^2 + \sigma_{1,y}^2 \\ \vdots & \vdots & \ddots & \vdots & \vdots \\ \sigma_{N-2,y}^2 & \sigma_{1,x}^2 + \sigma_{N-2,y}^2 & \cdots & \sigma_{N-2,x}^2 + \sigma_{N-2,y}^2 & \sigma_{N-1,x}^2 + \sigma_{N-2,y}^2 \\ \sigma_{N-1,y}^2 & \sigma_{1,x}^2 + \sigma_{N-1,y}^2 & \cdots & \sigma_{N-2,x}^2 + \sigma_{N-1,y}^2 & \sigma_{N-1,x}^2 + \sigma_{N-1,y}^2 \end{bmatrix} - \lambda,$$

u is defined on a squared $N \times N$ domain. The solution of the initial inhomogeneous modified Helmholtz equation is thus calculated as

$$u = C^\top ((CFC^\top)./M)C$$

using discrete cosine transform.

4 Numerical Results

For the numerical results, we consider the two different cases of surface reconstruction, namely, the 3D cartoon generation and the three dimensional map reconstruction, where in the first case we are given normal vectors along strokes while in the second case we are given both normal vectors and elevation data along contours and isolated points. The numerical tests are done using the augmented Lagrangian algorithm, Algorithm 1-2. Algorithm 1 is stopped when the total energy stabilized. For Algorithm 2, it was enough to use only one iteration.

In the cartoon case, we start with normal vectors along the strokes, which are given by artists. The results are shown in Fig. 1. Since we do not have the elevation data I_0, we set $\theta = 0$. In these experiments, we do not have flat surfaces, and hence

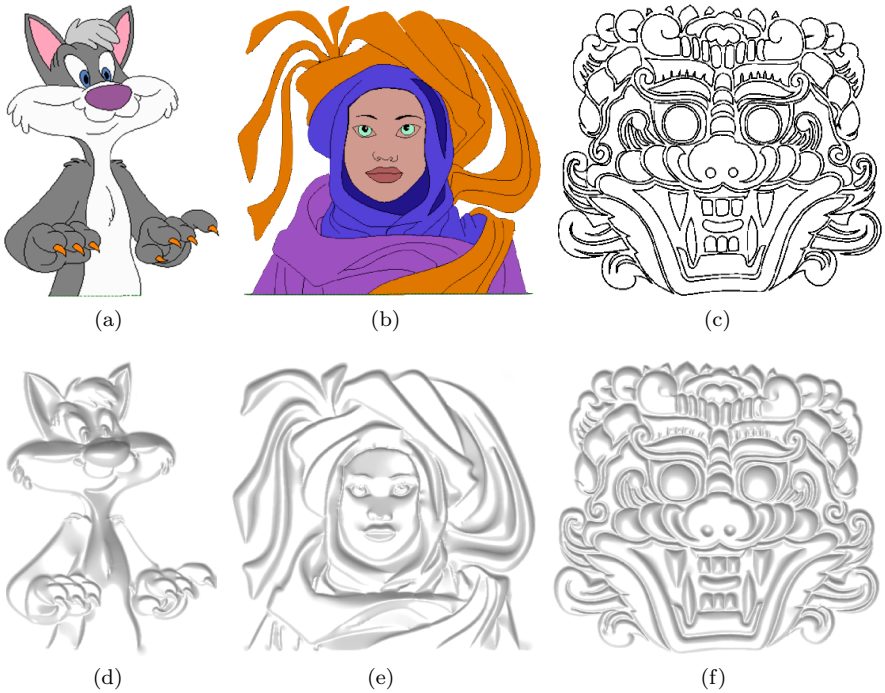

Fig. 1 Illustrating the cartoon case, where the input data are vectors along strokes (the top row) drawn by artists. The vectors are not shown here. The corresponding 3D cartoons generated by our algorithm, are shown in the bottom row. The parameters are $g = 0.5$, $h = 0$, $\theta = 0$, and $\eta = 5.0$.

we set $h = 0$. For flat surfaces h needs to be nonzero. We have used $g = 0.5$ and $\eta = 5.0$. As we can see from the Fig. 1, the algorithm is effective in preserving both structures and details.

In our next experiment with cartoon, we investigate the effect of the second order regularization by varying the g. The results are shown in Fig. 2, where the strokes and the normal vectors along the strokes are kept the same. θ is set equal to 0 in the experiment since the initial elevation is not known. h is set equal to 0 as we do not expect flat structures. The parameter g varies from 0.01 to 2.0 and the parameter η stays fixed at 5.0. As we can see in Fig. 2, the edges get sharper as g grows.

In our next experiment, we consider the 3D surface reconstruction of maps. The input data includes contours with height values, and isolated points with normal vectors. Fig. 3 presents the results with two different sparsities of input data, respectively 5.18% and 2.38%. The given normal vectors are kept the same for both cases, and are represented by the blue points, as shown in Fig. 3 (c) − Fig. 3 (d). The case in Fig. 3 (d) has much less information on elevation than the case in Fig. 3 (c), represented by the red points. The parameters for both cases are $g = 0.1$, $h = 0$, $\theta = 10^5$ and $\eta = 10^6$. The results show that, if we have adequate vector information, even with less height data, our model preserves the main feature of the 3D maps perfectly.

(a) g = 0.01 (b) g = 0.1 (c) g = 0.5

(d) g = 1 (e) g = 1.5 (f) g = 2

Fig. 2 Illustrating the effect of the second order regularization by varying the parameter g. In these tests, $h = 0$, $\theta = 0$, and $\eta = 5.0$.

In Fig. 4, we compare the effect of using vector constraint. Fig. 4 (a) shows the result of using the hybrid constraint while Fig.4 (b) shows the result using only the elevation data constraint. As we can see that without the vector constraint, in this test case, there is some loss of structure in the valley. The test cases in Fig. 4 (a) and Fig. 4 (b) have the same input points. The test case in Fig. 4 (b) has only elevation data as input, while in the test case in Fig. 4 (a) the elevation data is replaced with normal vectors for some points. Fig. 4 (d) the same reconstruction is made using the method [33] which is based on 3rd order anisotropic regularization. As we can see that our method manages to preserve the small structure comparatively better even with sparser data, because we have the flexibility to input additional information to our model like the normal vectors.

In the final experiment, cf. Fig. 5, the effect of the first order regularization is studied. As seen in the figure, the groundtruth contains a flat valley, cf. Fig. 5 (a) and Fig. 5 (d). The parameters g, η and θ are kept the same in the whole experiment, whose values are $g = 0.1$, $\eta = 0$ and $\theta = 10^6$. In Fig. 5 (b) and Fig. 5 (e), $h = 100$ while in Fig. 5 (c) and Fig. 5 (f) $h = 0$. As seen from the figure that ∇I term is needed to preserve the flat valley structure.

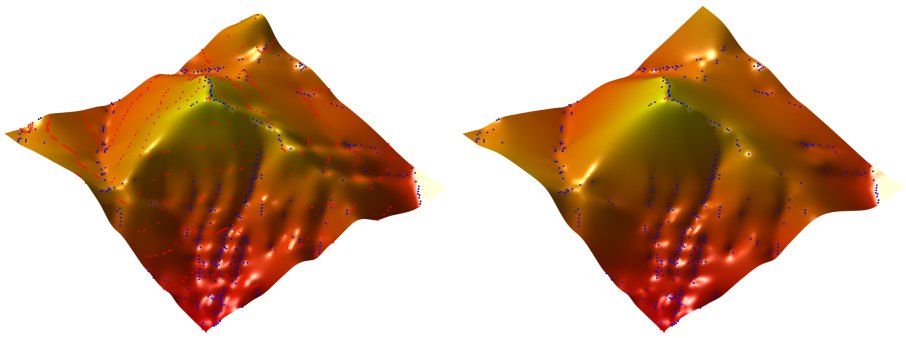

(a) Reconstructed surface corresponding to sparsity of Figure (c)

(b) Reconstructed surface corresponding to sparsity of Figure (d)

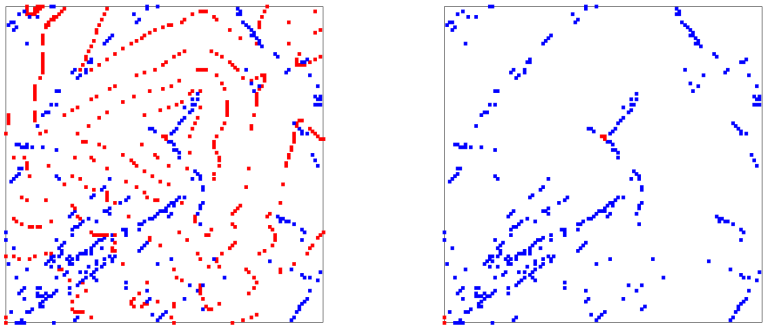

(c) Input data sparsity: 5.18%

(d) Input data sparsity: 2.38%

Fig. 3 3D surface reconstructions with two different sparsities of input data. Height values are given at red points, and normal vectors are given at blue points.

5 Conclusion

We have proposed a model for 3D surface reconstruction based on 2D sparse hybrid data, that is involving both height values and normal vectors in the same model, allowing for flexible control of their fidelity. An effective algorithm based on the augmented Lagrangian has been developed, where we split the minimization problem into six sub minimization problems, each with either a closed form solution or a fast solver. The proposed model is well suited for both 3D cartoon design and digital 3D elevation maps. Because it allows for flexible use of both the height data and the vector information, which can be on sparse curves or points, it has the potential to be used in areas where precise reconstruction of surfaces, represented by rather sparse data, are needed, and rather quick, for instance in real time applications like the web-based 3D visualization of maps, 3D GPS navigation, and 3D online gaming.

Acknowledgements XC Tai acknowledges the support from Norwegian Research Council through ISP-Matematikk (Project no. 239033/F20). The authors also thank Dr. Jie Qiu for providing us example strokes.

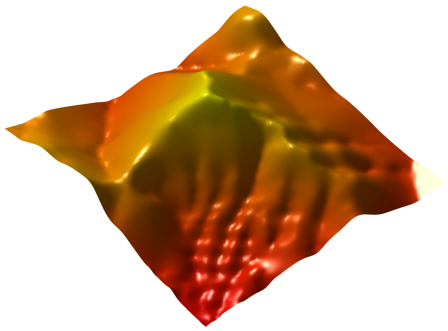

(a) Algorithm 1 and 2; hybrid constraint; input sparsity 5.24%

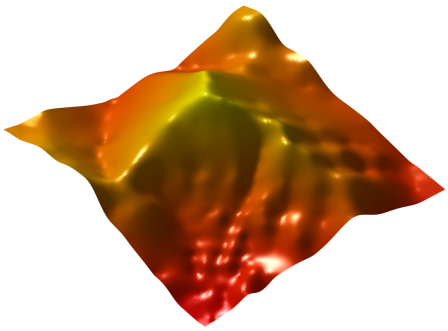

(b) Algorithm 1 and 2; elevation constraint; input sparsity 5.24%

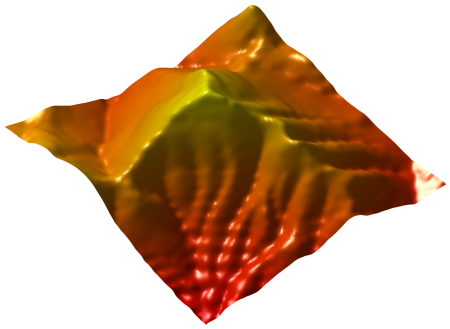

(c) The groundtruth

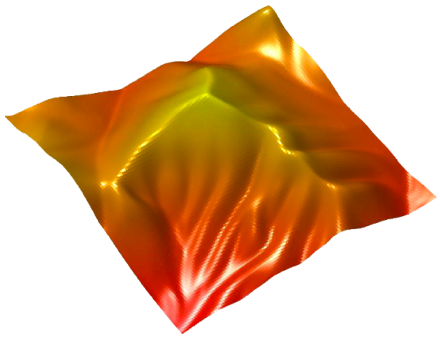

(d) Algorithm of [33]; elevation constraint on contours; input sparsity 7.42%

Fig. 4 Figures showing 3D reconstructions of map using different fidelity constraints, both elevation and vector constraint (hybrid) in Figure (a), only elevation constraint in Figure (b), using our algorithm, and elevation constraint on contours using the algorithm of [33] in Figure (d).

References

1. R. C. Zeleznik, K. P. Herndon, and J. F. Hughes. 1996. Sketch: an interface for sketching 3d scenes. The 23rd annual conference on Computer graphics and interactive techniques, pp. 163-170.
2. T. Igarashi, S. Matsuoka, and H. Tanaka. 1999. Teddy: a sketching interface for 3d freeform design. The 26th annual conference on Computer graphics and interactive techniques, pp. 409-416.
3. O. A. Karpenko and J. F. Hughes. 2006. SmoothSketch: 3D free-form shapes from complex sketches. The 33th annual conference on Computer graphics and interactive techniques, pp. 589-598.
4. A. Nealen, T. Igarashi, O. Sorkine, and M. Alexa. 2007. FiberMesh: designing freeform surfaces with 3D curves. ACM Transactions on Graphics, vol. 26, no. 3, p. Article No. 41.
5. L. Olsen, F. F. Samavati, M. C. Sousa, and J. A. Jorge. 2009. Sketch-based modeling: A survey. Computers & Graphics, vol. 33, no. 1, pp. 88-103.
6. Y. Gingold, T. Igarashi, and D. Zorin. 2009. Structured annotations for 2d-to-3d modeling. ACM Transactions on Graphics, vol. 28, no. 5, p. Article No. 148.

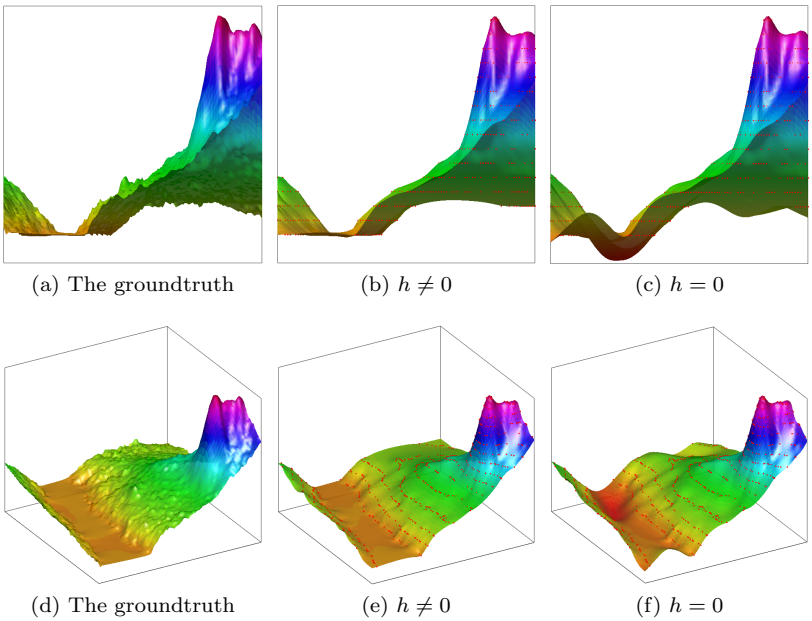

(a) The groundtruth (b) $h \neq 0$ (c) $h = 0$

(d) The groundtruth (e) $h \neq 0$ (f) $h = 0$

Fig. 5 Illustrating the effect of the first order regularization, 3D figures in the bottom row and 2D projection (yz-plane) in the top row. Inside the valley, we set the parameter h to 0 (switching off the first order regularization) in figures (c) and (f), and to 100 (switching it on) in figures (b) and (e). $h = 0$ in the rest of the domain. The sparsity of the input data is 5.98%. Here $g = 0.1$, $\eta = 0$, and $\theta = 10^6$ in all cases.

7. L. Olsen, F. F. Samavati, M. C. Sousa, and J. A. Jorge. 2005. Sketch-based mesh augmentation. The 2nd eurographics workshop on sketch-based interfaces and modeling.
8. J. Hahn, J. Qiu, E. Sugisaki, L. Jia, X.-C. Tai, and H. Seah. 2012. 6. Stroke-based surface reconstruction. CAM Report 12-18, UCLA.
9. J. Hahn, J. Qiu, E. Sugisaki, L. Jia, X.-C. Tai, and H. Seah. Stroke-based surface reconstruction. Numerical Mathematics: Theory, Methods and Applications, 6(1), 297-324, 2013.
10. A. Agrawal, R. Raskar, and R. Chellappa. 2006. What is the Range of Surface Reconstructions from a Gradient Field?. Computer Vision C ECCV, pp. 578-591, 2006.
11. R. T. Frankot, R. Chellappa, and S. Member. 1987. A Method for enforcing integrability in shape from shading algorithms. IEEE Transactions on Pattern Analysis and Machine Intelligence, pp. 118-128.
12. N. Petrovic, I. Cohen, B. J. Frey, R. Koetter, and T. S. Huang. 2001. Enforcing integrability for surface reconstruction algorithms using belief propagation in graphical models. Computer Vision and Pattern Recognition, IEEE Computer Society Conference on, vol. 1, p. 743.
13. T. Simchony, R. Chellappa, and M. Shao. 1990. Direct analytical methods for solving poisson equa- tions in computer vision problems. IEEE Transactions on Pattern Analysis and Machine In- telligence, vol. 12, pp. 435-446.
14. L. Zhang, G. Dugas-Phocion, and J.-S. Samson. 2002. Single-view modeling of free-form scenes. The Journal of Visualization and Computer Animation, vol. 13, pp. 225-235.
15. T.-P. Wu, C.-K. Tang, M. Brown, and H.-Y. Shum. Shapepalettes: Interactive normal transfer visa sketching. ACM Transactions on Graphics volumn 26 Issue 3 07, p. Article No.44.
16. M. Prasad and A. Fitzgibbon. 2006. Single view reconstruction of curved surfaces. The 2006 IEEE Computer Society Conference on Computer Vision and Pattern Recognition - Volume 2, pp. 1345-1354.

17. H.-S. Ng, T.-P. Wu, and C.-K. Tang. 2009. Surface-From-Gradients Without Discrete Integrability Enforcement: A Gaussian Kernel Approach. IEEE Transactions on Pattern Analysis and Machine Intelligence.
18. T. Rahman, X.C. Tai and S. Osher. 2007. A TV-Stokes Denoising Algorithm, Scale space and variational methods in computer vision. Springer Berlin Heidelberg, 473-483.
19. C.A. Elo, A. Malyshev and T. Rahman. 2009. A Dual Formulation of the TV-Stokes Algorithm for Image Denoising, Scale Space and Variational Methods in Computer Vision. Springer Berlin Heidelberg, 307-318.
20. Tai, X. C., Borok, S., Hahn, J.. 2009. Image denoising using TV-Stokes equation with an orientation-matching minimization. In International Conference on Scale Space and Variational Methods in Computer Vision (pp. 490-501). Springer Berlin Heidelberg.
21. Hahn, J., Tai, X. C., Borok, S., and Bruckstein, A. M.. Orientation-matching minimization for image denoising and inpainting. International journal of computer vision, 92(3), 308-324, 2011.
22. W.G. Litvinov, T. Rahman and X.C. Tai. 2011. A Modified TV-Stokes Model for Image Processing, SIAM Scientific Computing, 33(4): 1574-1597.
23. S. F. Johnston. 2002. Lumo: illumination for cel animation. The 2nd international symposium on Non-photorealistic animation and rendering. New York, NY, USA: ACM, pp. 45-52.
24. D. Meyers, S. Skinner, and K. Sloan. 1992. Surfaces from contours. Trans. on Graphics, 11(3):228-258.
25. S. Masnou and J. Morel. 1998. Level lines based disocclusion. In 5th IEEE International Conference on Image Processing, Chicago, IL, Oct. 4-7, pages 259-263.
26. T. Meyer. 2011. Coastal elevation from sparse level curves. Summer project under the guidance of T. Wittman, A. Bertozzi, and A. Chen, UCLA.
27. L. Alvarez, F. Guichard, P. L. Lions, and J. M. Morel. 1993. Axioms and fundamental equations of image processing. Arch. Rational Mech., 123:199-257.
28. V. Caselles, J.-M. Morel, and C. Sbert. 1998. An axiomatic approach to image interpolation. Trans. Image Proc., 7(3):376-386.
29. R. Franke. 1982. Scattered data interpolation: Test of some methods. Math. Comput.,38: 181-200.
30. J. Meinguet. 1984. Approximation Theory and Spline Functions, chapter Surface Spline Interpolation: Basic Theory and Computational Aspects, pages 124-142. Dordrecht, Holland.
31. J. C. Carr, W. R. Fright, and R. K. Beatson. 1997. Surface interpolation with radial basis functions for medical imaging. Trans. Med. Imaging, 16(1):96-107.
32. L. Mitas and H. Mitasova. 1999. Spatial Interpolation. Wiley.
33. J. Lellmann, J. M. Morel and C.-B. Schönlieb. 2013. Anisotropic Third-order Regularization for Sparse Digital Elevation Models, Springer Berlin Heidelberg.
34. Glowinski, R.,and Le Tallec, P. (1989). Augmented Lagrangian and operator-splitting methods in nonlinear mechanics. Society for Industrial and Applied Mathematics.
35. X.-C. Tai and C. Wu. 2009. Augmented Lagrangian method, dual methods and split Bregman iteration for ROF model. in SSVM, ser. Lecture Notes in Computer Science, X.-C. Tai, K. Mrken, M. Lysaker, and K.-A. Lie, Eds., vol. 5567. Springer, pp. 502?513.
36. C.L. Wu, J. Y. Zhang, and X.C. Tai. 2011. Augmented Lagrangian method for total variation restoration with non-quadratic fidelity. Inverse problems and imaging 5.1, 237-261.
37. Wang, Y., Yang, J., Yin, W., and Zhang, Y. (2008). A new alternating minimization algorithm for total variation image reconstruction. SIAM Journal on Imaging Sciences, 1(3), 248-272.
38. Meyer, C. D. (2000). Matrix analysis and applied linear algebra (Vol. 2). Siam.
39. Van Loan, C. (1992). Computational frameworks for the fast Fourier transform. Society for Industrial and Applied Mathematics.
40. C.A. Elo. (2009). Image Denoising Algorithms Based on the Dual Formulation of Total Variation. Master thesis. University of Bergen.